Symposium: Applications of Inorganic Photochemistry

Energy Conversion Chemistry: Mechanisms of Charge Transfer at Metal-Oxide Semiconductor/Solution Interfaces

Susan G. Yan, L. Andrew Lyon, Buford I. Lemon, Janice S. Preiskorn, and Joseph T. Hupp*
Department of Chemistry and Materials Research Center, Northwestern University, Evanston, IL 60208

One of the most promising strategies for chemistry-based solar energy conversion (light-to-electrical energy conversion) is the semiconductor/liquid junction solar cell (*1*). The strategy can involve direct collection of light by the semiconductor, where the requirement for light collection is photonic energy that exceeds the gap in energy between the valence band and the conduction band (Fig. 1a; see also the accompanying article by Meyer). When this occurs an electron is promoted from the valence band to the (empty) conduction band, leaving behind a positively charged valence-band vacancy or hole. One of the particles (typically the hole) migrates to the semiconductor/solution interface, where it can oxidize a molecule in solution. The electron, on the other hand, moves away from the interface and toward an external circuit, where some of its free energy can be extracted before it reaches a dark electrode. At the dark electrode the circuit is completed: the electron is captured by an oxidized molecule that has diffused through solution from the illuminated semiconductor electrode. Note that in this scheme no *net* chemical reaction occurs; every interfacial oxidation reaction is offset by an interfacial reduction reaction, and only electricity is produced.

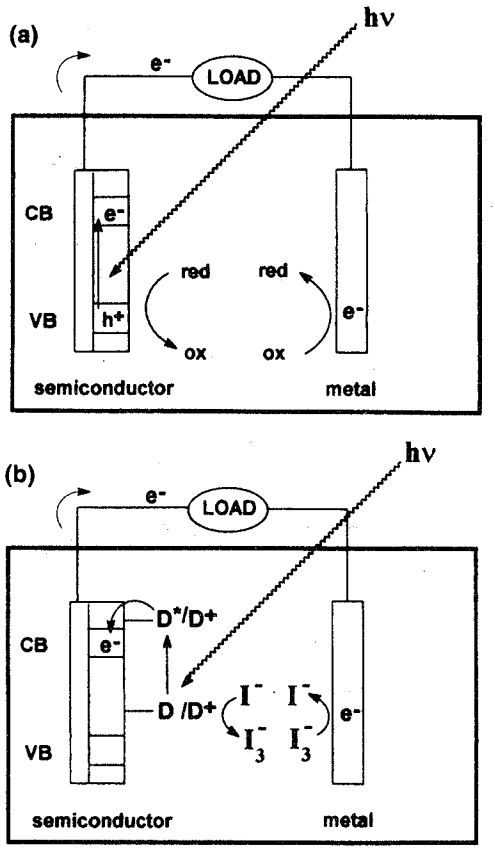

Figure 1. (a) Schematic representation of a semiconductor/liquid junction photovoltaic cell where VB is the valence band, CB is the conduction band, e^- is an electron, h^+ is a hole (electron vacancy) and red and ox represent the reduced and oxidized forms of a solution redox species. (b) Schematic of a dye-sensitized photovoltaic cell where D represents the surface-bound dye and the specific solution redox species is the I^-/I_3^- couple. All other symbols have the same meaning as in Figure 1 (a).

*Corresponding author

The "direct" energy conversion strategy clearly is best suited to semiconductor materials that can absorb significant portions of the solar spectrum—that is, materials with bandgaps of ca. 1 to 2 eV.[1] Unfortunately, many materials with acceptable bandgaps are susceptible to destructive hole-based reactions. For example, chalcogenide-based compound semiconductors such as cadmium selenide efficiently photocorrode, yielding soluble metal cations and polychalcogenide species (*2*). Other materials, such as silicon and indium phosphide, can react with water or oxygen to generate electrically insulating barrier layers (*3*).

Alternative materials based on metal oxides are typically kinetically resistant to photocorrosion but exhibit bandgaps too large to permit significant collection of visible light (i.e., light of 400–700 nm wavelength). (For example, the bandgap, E_{BG}, for TiO_2 (anatase) is 3.2 eV, yielding an absorption onset of ca. 380 nm.) As shown in Figure 2, however, wide-bandgap semiconductors can be converted into visible-light absorbers by coating them with visible light–absorbing dye molecules (*4*). Here light absorption promotes an electron from the highest-occupied molecular

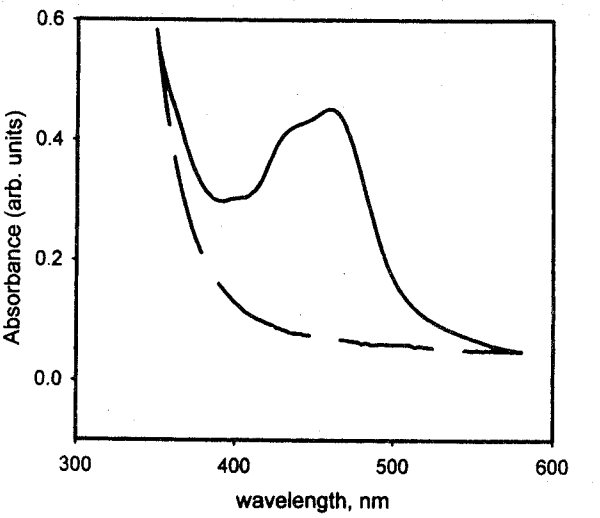

Figure 2. Electronic absorption spectrum of colloidal TiO_2 sensitized with a RuL_3 dye. Broken line shows absorbance spectrum without dye.

orbital (HOMO) to the lowest-unoccupied molecular orbital (LUMO) of the dye. The resultant high-energy electron can cross the semiconductor/solution interface and enter the conduction band. As in Figure 1a, the conduction band electron can exit from the semiconductor, do electrical work, and move on to a dark electrode. Note that the initial electron injection reaction leaves the dye in its oxidized (transparent) form. The dye, however, can react with a solution-phase reductant and be restored to its light-absorbing form. The solution species then diffuses to the dark electrode, where it can combine with an electron to complete the circuit.

The viability of energy conversion schemes based on semiconductor/liquid junction interfaces depends, in large part, on the efficacy of forward electron transfer reactions and the inhibition of reverse reactions (*1,4,5*). The purpose of this paper is to discuss mechanisms of electron transfer specifically at metal-oxide semiconductor/solution interfaces. The focus is on the energetic, kinetic, and structural factors associated with optimal energy conversion. The discussion is motivated by a number of new experiments involving both light and dark semiconductor/solution interfaces. As in many experimentally active areas of chemistry, the corresponding theory is in an interesting state of flux. The *interpretation* of new experiments, therefore, is necessarily speculative.

Background: Branching Ratios, Conversion Efficiencies, and Electron Transfer Kinetics

Efficient energy conversion begins with efficient light absorption, followed by efficient dye-to-semiconductor electron transfer. Both are routinely achievable with nanocrystalline metal-oxide materials when these are configured in high-area, thin-film form (*1a, 4a, 4b*). After injection the electron can either move through the film, reach an external circuit and do electrical work, or return to the surface-bound dye in an energy-wasting back reaction. The competitive branching ratio for this pair of processes is one of several that must be large in order for overall energy conversion to occur effectively.

It is important to appreciate that essentially all the branching ratios are kinetically controlled. For the ratio discussed above, the most relevant kinetics are those for back electron-transfer (back ET) and for yet another competitive reaction: capture of the oxidized dye by a solution-phase electron relay such as the I^-/I_3^- couple (*6*) (Fig. 1b). (Note that successful capture eliminates the possibility of back ET, leaving the desired film transport process as the default reaction pathway.) As one might expect, the half-life for the capture reaction depends on the concentration of the reduced form of the redox relay, higher relay concentrations yielding shorter half-lives. Empirically, the briefest half-lives for capture of oxidized inorganic dyes on high-area metal-oxide semiconductor surfaces are on the order of 20 ns (*7*). It follows that the branching ratio will be suitably large if the half-life for back ET is ca. 80 ns or longer (branching ratio > 0.75).[2] Because this particular branching ratio is both difficult to control and mechanistically important, we will focus most of our attention on the crucial back ET process.

The kinetics for back ET are generally complex. A typical kinetic trace, based on transient absorbance monitoring of a surface bound dye, is shown in Figure 3. Following rapid bleaching caused by both photoexcitation and electron injection, the ground state dye absorbance is recovered in (i) an approximately first-order process that is comparatively rapid, and (ii) a more complicated process requiring additional time and likely involving one or more shallow trap

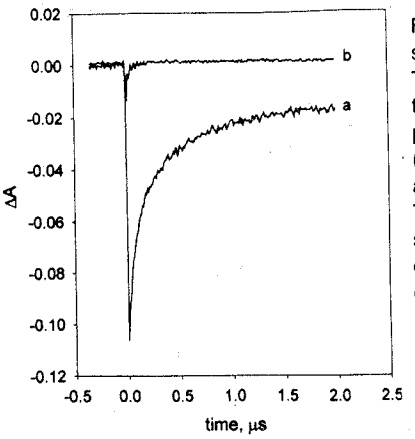

Figure 3. Transient absorbance signals for TiO_2 colloid sensitized with $Ru^{II}L_2$(5-Cl-phen) without added I^- (curve *a*) and with added I^- (curve *b*). The short half-life observed in curve *b* is due to the rapid reduction of $Ru^{III}L_2$(5-Cl-phen) by I^-.

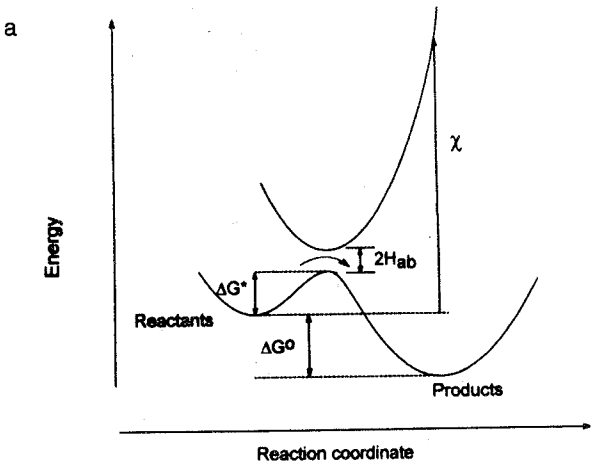

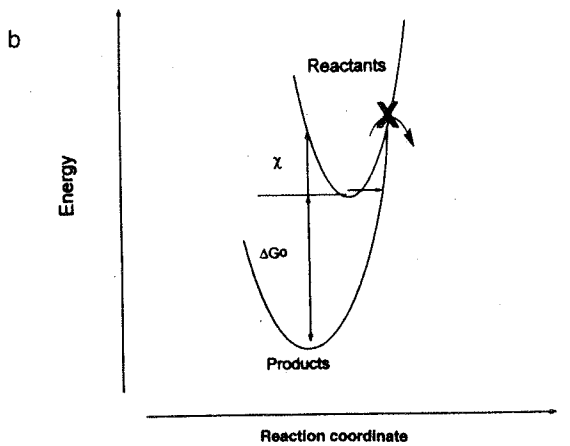

Figure 4. (a) Potential energy surfaces depicting activated electron transfer in the Marcus normal region. ΔG^* is the activation free energy, χ is the reorganization energy, ΔG° is the reaction driving force, and H_{ab} is the electronic coupling between initial state, *a*, and the final state, *b*. (b) Potential energy surfaces for Marcus inverted region behavior observed when the absolute value of the thermodynamic driving force exceeds the kinetic reorganization energy. Electron transfer now occurs via surface-to-surface tunneling.

sites (*8*). (Trap sites are localized chemical defect/redox sites capable of transiently retaining injected electrons.) Because the first process is more rapid and is almost certainly simpler to interpret, we will focus on it and ignore, for now, the more complex kinetics occurring at later time.

Conventional wisdom holds that Marcus-type electron transfer theory (*9*) is applicable to the back ET process (*1*). If one assumes that ET occurs from a localized surface redox site, the first-order electron transfer rate constant can be written as:

$$k_{ET} = f(H_{ab}^2) \cdot FCWD \qquad (1)$$

The first part of the equation characterizes the effective frequency factor for electron transfer and depends on the extent of electronic coupling (H_{ab}) between the initial state, *a*, with the electron in the semiconductor, and the final state, *b*, with the electron in the dye molecule. The second part of the equation, the "Franck–Condon weighted density of states" (*FCWD*), describes the role played by nuclear (vibrational and solvational) coordinate displacements. In the classical limit, for weakly or moderately exothermic reactions, the *FCWD* term behaves as an Eyring activation free energy term; that is, $FCWD \approx \exp(-\Delta G^*/RT)$. As shown in Figure 4a, the magnitude of the activation free energy should depend on the sizes of both the reorganization energy, χ, and the reaction driving force, $\Delta G°$. According to the Marcus theory, the reorganization energy is large when coordinate displacements are large and small when coordinate displacements are small (*9*). The reaction free energy is given nominally by the difference in formal potential between the dye redox couple and the semiconductor-localized redox site. Or, if the electron is delocalized within the semiconductor, then the relevant potentials are the dye formal potential, E_f(dye), and the conduction band edge, E_{CB}. In either case, the *FCWD* term—and therefore, the rate constant—should increase as the driving force increases and also as the temperature increases.

In contrast, if the driving force is large (Fig. 4b; $\chi < -\Delta G°$), the *FCWD* term behaves as an activationless tunneling term (*9*). The experimental manifestation of the tunneling effect is an approximate temperature independence for the ET rate constant. Curiously, under these conditions the term becomes smaller and the ET rate constant *decreases* as the reaction driving force increases. In the electron transfer literature this interesting phenomenon is known as "inverted" reactivity and can be contrasted with the "normal region" behavior expected under less exothermic conditions; see Figure 4 (*9*). If the theory is applicable here, then systematic studies of overall cell performance—or better yet, isolated electron transfer reaction kinetics—as functions of $\Delta G°$ and temperature should be highly diagnostic of ET mechanism and should provide direct insight into chemical factors determining efficiency.

Mechanistic Studies: Back Reaction Pathways

One of the more unusual features of photoelectrochemical cells based on inorganic dyes and metal-oxide semiconductors is their comparatively high power-conversion efficiencies: values as high as 10% have been claimed (*10*). As suggested above, high efficiencies are associated with large branching ratios and sluggish kinetics for energy-wasting back ET reactions (*1, 4, 5*). Our recent work has focused on the back ET problem with particular emphasis on driving-force effects. Figure 5 shows an example of semiconductor (titanium dioxide)-to-dye back ET reactivity where the reaction driving force has been tuned by tuning the formal potential of the dye. The dyes comprise chelate (bipyridine and phenanthroline) complexes of ruthenium (II) (*6*). Carboxylate substituents on the bipyridyl ligand anchor the dyes to the semiconductor surface, presumably via Ti(IV) chelation. As shown in eq 2, light absorption occurs via metal-to-ligand charge transfer. Forward ET ("injection") occurs from the ligand radical anion present in the dye excited state. Back ET, on the other hand, involves reduction of the oxidized metal ion [Ru(III)] located at the center of the dye (*1, 6*). In this experiment, the potential of the Ru(III/II) couple and the driving force for back ET are adjusted via inductive effects associated with substituents on the phenanthroline ligands (*11*).

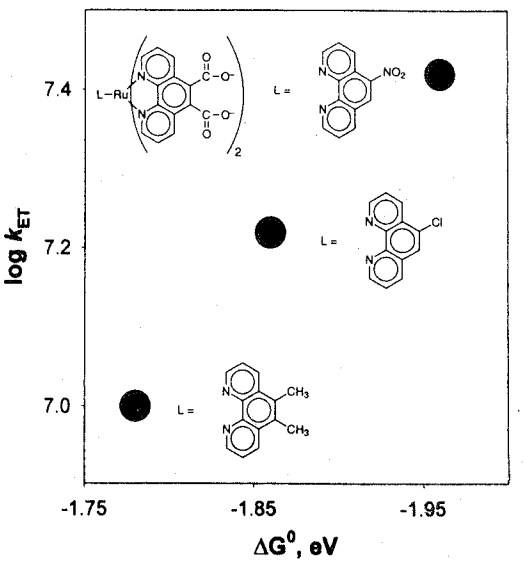

Figure 5. Variation of the back ET rate with overall reaction driving force ($\Delta G°$). The driving force is tuned by changing the $Ru^{III/II}$ formal potential in the dye via inductive substituent effects on the phenanthroline. The faster rate with larger driving force indicates that the reaction is occurring in the Marcus normal region.

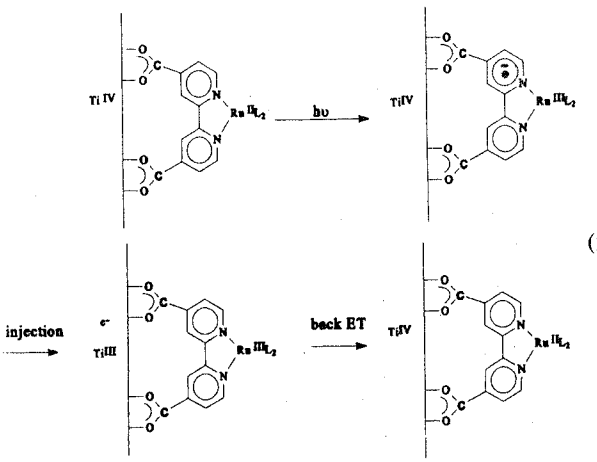

(2)

The important observations are that (i) forward ET occurs rapidly (less than 5 ns half-life; data not shown); (ii) back ET occurs less rapidly (ca. 50–200 ns half-life); (iii) back ET rates increase as the reaction driving force in-

creases. From Figure 6 and the discussion above, back ET occurs in the Marcus normal region. It follows that back ET is slow, in part, because of the need to surmount an activation barrier (see Fig. 4a). Variable temperature kinetics confirm that back ET is thermally activated.[3] The variable temperature experiments also reveal, however, that the kinetics are slowed by poor electronic coupling (i.e., small H_{ab} term in eq 1). In retrospect, this is not surprising, given the need for the transferring electron to traverse 7 bonds in the back reaction.[4] In contrast, the much faster forward ET process requires coupling or communication through just 3 bonds (see eq 2). Thus, the electronic asymmetry of the forward and reverse reactions appears to account for some of the rate disparity. Returning to the driving force observations, these *are* surprising. From Figure 4b, they require that the reorganization energy for ET significantly exceed the driving force for ET. The difficulty is that the Ru(III/II) couple is known to pose little in terms of internal reorganizational demands (*12*). Indeed, even accounting for possible semiconductor lattice (*13*) and external solvent reorganizational (*14*) contributions, the total reorganization energy almost certainly is less than 1 eV (23 kcal/mol). The overall reaction driving force, on the other hand, is ca. -2 eV, implying that back reactions ought to occur instead in the Marcus inverted region (*9, 15*).

An alternative strategy for varying driving forces is to exploit the well known "Nernstian" dependence of E_{CB} for metal-oxide semiconductors on solution pH (i.e. -60 mV shift in E_{CB} per pH unit) (*16*). Figure 6b summarizes the results of an experiment in which back ET from titanium dioxide to a hexaphosphonated ruthenium dye was examined over a range of 19 pH units. (Substitution of phosphonate groups for carboxylate groups is necessary to sustain surface binding under extreme pH conditions.) The redox potential of the surface-bound dye is not pH-dependent. The pH changes translate into enormous changes in overall reaction free energy (i.e., up to 1.1 eV or 26 kcal/mol). The remarkable finding in Figure 6b is that k_{ET} is independent of pH or driving force over the entire range, implying that neither inverted nor normal behavior is occurring (*8a*). Additional variable temperature experiments show, however, that the back reaction is thermally activated, suggesting that somehow the reaction is occurring in the Marcus normal region.

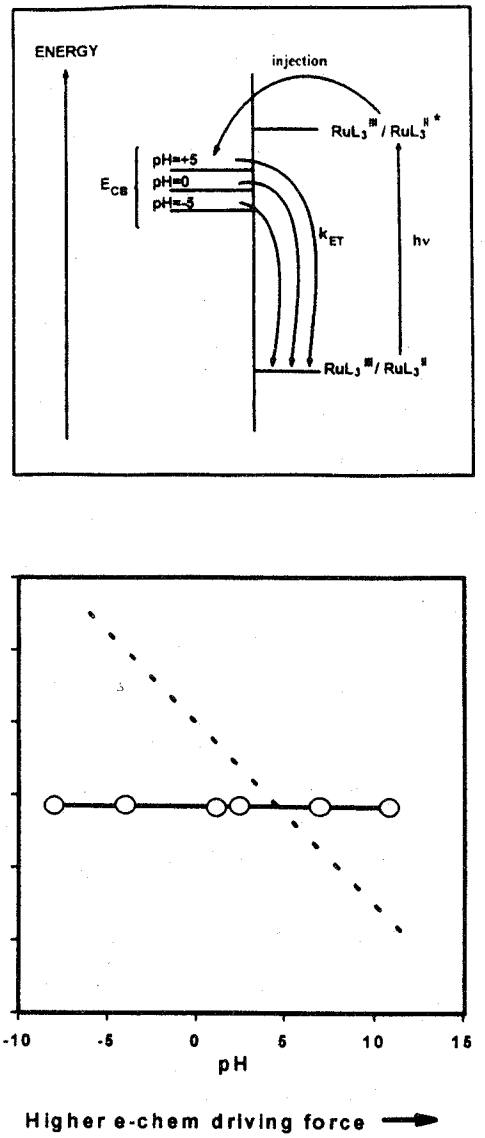

Figure 6. (a) Diagram representing change in overall reaction driving force with pH for forward and back ET. Driving force is varied here by tuning the conduction band edge energy (E_{CB}) with changes in solution pH while keeping the $Ru^{III/II}$ potential fixed. (b) Observed dependence of back ET rate constant (k_{ET}) on solution pH. The dashed line depicts hypothetical inverted region behavior.

Mechanistic Studies: Interfacial Energetics

In light of the unexpected insensitivity of back ET reactivity to semiconductor-based driving-force changes, it is worth asking how the changes in driving force or E_{CB} arise chemically. One explanation is that they reflect the ability to protonate or deprotonate the metal oxide/hydroxide surface. The accompanying changes in surface charge provide a coulombic basis for altering E_{CB}. One of the difficulties with this explanation is that it only accidentally yields Nernstian behavior—and then only over a narrow pH range. Another difficulty is that the energy shifts persist experimentally even in solutions where the surface is fully protonated or fully deprotonated (based on electrophoretic measurements of surface pK_a's for semiconductors in colloidal form) (*17*). Indeed, for TiO_2, Nernstian energy shifts persist through a pH range greater than 20 units.

An alternative but related interpretation for the energy effects centers on redox-induced proton intercalation effects. The pertinent experiments are quartz crystal microbalance (QCM) studies of nanocrystalline titanium dioxide electrodes. In these experiments, electrons are introduced electrochemically while the mass of the electrode is simulta-

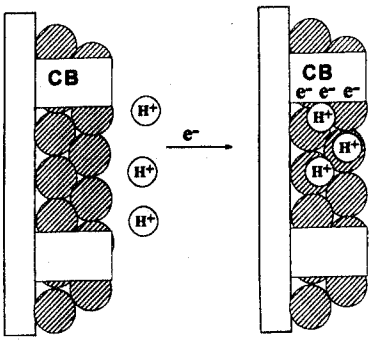

Figure 7. Representation of a nanocrystalline TiO_2 film under "accumulation" conditions where each excess electron is accompanied by an intercalated proton from the solution. Symbols have the same meaning as in Figure 1.

neously monitored. The basic finding is that for every electron added a proton is intercalated (*18*), as shown schematically in Figure 7 and in the following reaction sequence:

$$TiO_2 + e^-(\text{external}) + H^+(\text{solution}) \rightarrow Ti(O)(OH)\cdot e^-_{CB} \quad (3)$$

Or, if a more localized description is preferred:

$$Ti^{IV}O_2 + e^-(\text{external}) + H^+(\text{solution}) \rightarrow Ti^{III}(O)(OH) \quad (4)$$

We note that similar behavior occurs at tin-oxide/water and zinc-oxide/water interfaces (*19*). It also occurs under photochemical conditions when a chemical scavenger is present in solution for hole capture (*20*). In any case, the reversible coupling of electron "accumulation"[5] to proton uptake leads in a straightforward way to a Nernstian dependence of E_{CB} on pH. The pH dependence will persist until the solution is either so acidic that intercalation can occur without electron addition, or so basic that intercalation is impossible even in the presence of the added electron. Our preliminary studies indicate that the former occurs at an effective pH of ~8.5 and below and that the latter occurs only at pH's of 23 and above.[6]

Mechanistic Speculations

The available mechanistic observations and conclusions are the following.

1. Slow back ET is a consequence of activated reactivity in the Marcus normal region and poor electronic coupling.
2. The back reaction rate constant, however, is insensitive to semiconductor-based changes in apparent driving force.
3. The overall reaction driving force exceeds the reorganization energy.
4. Electron accumulation is coupled to proton transfer.
5. The coupling provides an alternative explanation for the Nernstian dependence of conduction band edge energetics on solution pH.

Conclusions 4 and 5 suggest a means of reconciling the apparent conflict between the first observation and observations 2 and 3. The key is to distinguish carefully between the overall energetics for coupled proton transfer/electron transfer[7] and the energetics for electron transfer in isolation. Only the latter is directly relevant in Marcus-type treatments of reaction kinetics, but only the former is obtained from standard electrochemical thermodynamic measurements. To illustrate further, we suggest the following *sequential* electron transfer/proton transfer reaction scheme:

$$Ti^{IV}O_2 + Ru^{III}L_2L^{\cdot-} \rightarrow Ti^{III}O_2 + Ru^{III}L_3 \quad \text{(injection)} \quad (5)$$

$$Ti^{III}O_2 + H^+ \rightarrow Ti^{III}(O)(OH) \quad \text{(intercalation)} \quad (6)$$

$$Ti^{III}(O)(OH) + Ru^{III}L_3 \rightarrow Ti^{IV}(O)(OH) + Ru^{II}L_3 \quad \text{(back ET)} \quad (7)$$

$$Ti^{IV}(O)(OH) \rightarrow Ti^{IV}O_2 + H^+ \quad \text{(expulsion)} \quad (8)$$

In this scheme, the electron source for back ET to the molecular dye is a $Ti^{III}(O)(OH)$ species or a related electronically delocalized entity. For an isolated electron transfer reaction, its strength as a reductant is given (in the molecular limit) by the formal potential for the $Ti^{IV}(O)(OH)/Ti^{III}(O)(OH)$ couple; $\Delta G°$ for electron transfer (*only*) (eq 6) is then given by the difference between this potential and the formal potential of the dye. Note that this driving force is not pH dependent. The driving force for the overall back reaction (combined electron + proton transfer; eqs 7 and 8), on the other hand, is given by the difference between E_{CB} and the dye formal potential. As discussed above, this driving force is pH dependent. Except at extremely negative pH's, therefore, the two driving forces will differ. Furthermore, at moderate pH's the difference is substantial, and the driving force for the isolated electron transfer reaction is smaller.

If it is assumed that interfacial electron transfer rather than proton transfer is rate-determining, the proposed scheme predicts (i) large overall reaction driving forces, (ii) smaller electron-transfer driving forces that place the kinetics in the Marcus normal region, and (iii) insensitivity of reaction rates to changes in pH. The predictions are gratifying and appear to describe a number of metal-oxide semiconductor/dye back reactions of interest in solar energy conversion. Depending on the exact sequence of forward and reverse electron and proton transfer, however, other outcomes are possible, including pH-independent inverted region behavior and pH-variable normal or inverted behavior. Interestingly, examples of both already exist in the semiconductor photoelectrochemistry literature, albeit for molecular systems that differ both energetically and structurally from those described here (*21*). Presumably, as with other multistep reactions, the exact pathway followed depends primarily on optimization of the overall kinetics.

Conclusions

While the basic principles of dye-sensitized solar energy conversion have been understood for some time, the physical chemical basis for *efficient* sensitization of metal-oxide semiconductors is beginning to emerge from systematic studies of electron transfer kinetics and interfacial energetics. Although the detailed interpretation of new experiments is still in a state of flux, the available new results from our lab and several others offer some guidance in terms of enhanced chromophore design and solar cell efficiency optimization. The experiments also provide important new basic knowledge concerning charge transfer reactivity at light-sensitive electrochemical interfaces.

Acknowledgments

We thank the Office of Naval Research and the DOD AASERT program for support of our research. SGY acknowledges the Materials Research Science and Engineering Center at Northwestern (NSF DMR-9120521) for support as a University Graduate Fellow. LAL and JNP acknowledge fellowship support from the Link Foundation. LAL also acknowledges summer fellowship support from the Electrochemical Society.

Notes

1. Obviously, materials with still smaller gaps can collect even greater portions of the solar spectrum. Net power generation suffers, however, because only small photovoltages (necessarily less than the bandgap) can be generated.

2. Further increases in back ET half-life clearly will provide only small enhancements in branching ratio. Nevertheless, extended half-lives can lead to enhanced efficiencies because of increased photovoltages. See, for example, Argazzi, R.; Bignozzi, C. A.; Heimer, T. A.; Castellano, F. N.; Meyer, G. J. *J. Am. Chem. Soc.* **1995**, *117*, 11815–11816.

3. Variable temperature measurements were made on a hexaphosphonated analogue of $Ru(bpy)_3^{2+}$ as a substitute to the prototypical carboxylated dye. The phosphonated dye adsorbs

more strongly to the TiO_2 surface, allowing for higher loadings and a wider range of temperature and pH stability.

4. This is not to imply that the electron occupies each bond sequentially during back ET. Instead, the intervening bonds or orbitals serve to couple the electron donor and the electron acceptor in a virtual or superexchange sense.

5. The exact nature of the "band" structure of nanocrystalline semiconductor materials is still debated in the literature (e.g., Cao, F.; Oskam, G.; Searson, P. C.; Stipkala, J. M.; Heimer, T. A.; Farzad, F.; Meyer, G. J. *J. Phys. Chem.* **1995,** *99*, 11974–11980). Consequently, terms such as "accumulation layer" have less precise meanings than they would for more ideal materials. Here we use the accumulation term loosely to indicate the (energetic) conditions under which electrons can be electrochemically added to the unilluminated semiconductor film.

6. While simple proton concentrations corresponding to pH's below -2 and above +16 clearly are unphysical, proton *activities* in these ranges are not.

7. The term "proton coupled electron transfer" is sometimes reserved for simultaneous transfer (Roberts, J. A.; Kirby, J. P.; Nocera, D.G. *J. Am. Chem. Soc.* **1995,** *117*, 8051–8052). Here we use the term in a broader sense that also encompasses closely linked sequential reaction processes.

Literature Cited

1. For recent reviews see (a) Hagfeldt, A.; Grätzel, M. *Chem. Rev.* **1995,** *95*, 49–68; (b) Tan, M. X.; Laibinis, P. E.; Nguyen, S. T.; Kesselman, J. M.; Stanton, C. E.; Lewis, N. S. *Prog. Inorg. Chem.* **1994,** *41*, 21–144.
2. See, for example (a) Rosamilia, J. M.; Miller, B. *J. Electrochem. Soc.* **1985,** *132*, 349–353; (b) Wrighton, M. S. *Acc. Chem. Res.* **1979,** *12*, 303–310.
3. (a) Bolts, J. M.; Bocarsly, A. B.; Palazzotto, M. C.; Walton, E. G.; Lewis, N. S.; Wrighton, M. S. *J. Am. Chem. Soc.* **1979,** *101*, 1378–1385; (b) Heben, M. J.; Kumar, A.; Zheng, C.; Lewis, N. S. *Nature* **1989,** *340*, 621–623.
4. For reviews see (a) Kamat, P. V. *Chem. Rev.* **1993,** *93*, 267–300; (b) Meyer, G. J.; Searson, P. C. *Interface* **1993,** *2*, 23; (c) Parkinson, B. A.; Spitler, M. T. *Electrochim. Acta* **1992,** *37*, 943–948.
5. Lewis, N. S. *Acc. Chem. Res.* **1990,** *23*, 176–183.
6. Vlachopoulos, N.; Liska, P.; Augstynski, J.; Grätzel, M. *J. Am. Chem. Soc.* **1988,** *110*, 1216–1220.
7. Nazeeruddin, M. K.; Kay, A.; Rodicio, I.; Humphry-Baker, R.; Müller, E.; Liska, P.; Vlachopoulos, N.; Grätzel, M. *J. Am. Chem. Soc.* **1993,** *115*, 6382–6390.
8. (a) Yan, S. G.; Hupp, J. T. *J. Phys. Chem.* **1996,** *100*, 6867–6870; (b) Bedja, I.; Hotchandani, S.; Kamat, P. V. *J. Phys. Chem.* **1994,** *98*, 4133–4140; (c) Ford, W. E.; Rodgers, M. A. J. *J. Phys. Chem.* **1994,** *98*, 3822–3831; (d) Argazzi, R.; Bignozzi, C. A.; Heimer, T. A.; Castellano, F. N.; Meyer, G. J. *Inorg. Chem.* **1994,** *33*, 5741–5749.
9. (a) Marcus, R. A. *J. Chem. Phys.* **1965,** *43*, 679; (b) Sutin, N. *Prog. Inorg. Chem.* **1983,** *30*, 441; (c) Newton, M. D.; Sutin, N. *Annu. Rev. Phys. Chem.* **1984,** *35*, 437–480; (d) Scandola, F.; Balzani, V. *J. Chem. Educ.* **1983,** *60*, 814–823.
10. O'Regan, B.; Grätzel, M. *Nature* **1991,** *353*, 737–740.
11. Preiskorn, J. S. *Res. Rep. Link Energy Fellows* **1995,** *10*, 84–99.
12. Brown, G. M.; Sutin, N. *J. Am. Chem. Soc.* **1979,** *101*, 883–892.
13. Blackbourn, R. L.; Johnson, C. S.; Hupp, J. T. *J. Am. Chem. Soc.* **1991,** *113*, 1060–1062.
14. (a) Smith, B. B.; Koval, C. A. *J. Electroanal. Chem.* **1991,** *319*, 19–31; (b) Marcus, R. A. *J. Phys. Chem.* **1990,** *94*, 1050–1055.
15. Moser, J. E.; Grätzel, M. *Chem. Phys.* **1993,** *176*, 493–500.
16. (a) Rothenberger, G.; Fitzmaurice, D.; Grätzel, M. *J. Phys. Chem.* **1992,** *96*, 5983–5986; (b) Watanabe, T.; Fujishima, A.; Tatsuoki, O.; Honda, K.-I. *Bull. Chem. Soc. Jpn.* **1976,** *49*, 8–11; (c) Dutoit, E. C.; Cardon, F.; Gomes, W. P. *Ber. Bunsenges. Physik. Chem.* **1976,** *80*, 475–481.
17. Berube, Y. G.; Bruyn, D. *J. Colloid Interface Sci.* **1968,** *27*, 305–323.
18. Lyon, L. A.; Hupp, J. T. *J. Phys. Chem.* **1995,** *99*, 15718–15720.
19. Lemon, B. I.; Hupp, J. T. *J. Phys. Chem.*, in press.
20. Lemon, B. I.; Hupp, J. T. *J. Phys. Chem.* **1996,** *100*, 14578–14580.
21. (a) Moser, J.; Grätzel, M. *J. Am. Chem. Soc.* **1983,** *105*, 6547–6554; (b) Lu, H.; Prieskorn, J.; Hupp, J. T. *J. Am. Chem. Soc.* **1993,** *115*, 4927–4928.